CHEMISTRY OF MATERIALS
Article

Chem. Mater. **2011,** *23,* 945–952 945
DOI:10.1021/cm102082j

Low-Energy Path to Dense HfO_2 Thin Films with Aqueous Precursor

Kai Jiang,[†] Jeremy T. Anderson,[†] Ken Hoshino,[‡] Dong Li,[§] John F. Wager,[‡] and Douglas A. Keszler*[,†]

[†]*Department of Chemistry, Oregon State University, 153 Gilbert Hall, Corvallis, Oregon 97331-4003, United States,* [‡]*School of Electrical Engineering and Computer Science, 1148 Kelley Engineering Center, Oregon State University, Corvallis, Oregon 97331-5501, United States, and* [§]*ASM America, Inc., 3440 E. University Dr., Phoenix, Arizona 85034, United States*

Received July 26, 2010. Revised Manuscript Received November 11, 2010

New, stable aqueous solutions have been developed for the deposition of high-quality HfO_2 thin films. The low ionic strength of the solution relative to a stoichiometric salt provides the means to directly spin coat a film without organic additives. Peroxide mediates particle interaction in the solution, while enabling relatively low-energy pathways for condensation of the precursor species to a film. Film structure, chemistry, and density are investigated by X-ray diffraction, FT-IR, electron-probe microanalysis, SEM, and X-ray reflectivity. Results from these measurements collectively reveal that smooth and dense HfO_2 films are readily produced from the precursors with annealing at moderate temperatures. Optical properties of the films are studied by spectroscopic ellipsometry and transmission/reflection measurements. The observed refractive indices (1.89−1.93) are comparable to those achieved via vapor deposition techniques. Dielectric properties are evaluated through integration of the films into capacitors and thin film transistors. Performance as capacitor dielectrics is characterized by leakage current densities < 10 nA/cm^2 (at 1 MV/cm) and breakdown fields up to 5.5 MV/cm. As gate dielectrics in thin film transistors with amorphous indium gallium zinc oxide channels, the films exhibit small gate leakage, enabling transistor performance with incremental mobilities near 13 cm^2/V·s.

Introduction

HfO_2 thin films are widely used as coatings for laser optics[1,2] and as gate dielectrics in advanced transistor technologies.[3−5] To fulfill most application requirements, it is essential that the films be smooth and dense in a thickness range from < 10 to several hundred nanometers. Consequently, advanced vapor methods, such as electron beam evaporation,[6] chemical vapor deposition (CVD),[7,8] sputtering,[9,10] and atomic layer deposition (ALD)[11−13] have been favored for film deposition. Even with these sophisticated techniques, it can be challenging to produce films with the desired properties. For example, energy-assisted deposition is generally required to produce highly dense films for optics. Postdeposition anneals of dielectric films are often necessary to lower defect concentrations. Annealing, however, generally induces crystallization of HfO_2, producing in a dielectric unwanted grain boundaries, associated leakage current and impurity diffusion pathways, and surface or interfacial roughness, leading to thermal losses and poor device reliability. In many cases, the tolerable range of deposition conditions or "process window," is quite small. In addition, scaling vapor deposition of HfO_2 films to large areas with high uniformity remains problematic.[14]

High-speed printing or coating of thin film materials from solution precursors (inks) offers a potentially simple and low-energy opportunity for realizing large-area fabrication of electronic and electro-optical devices. Of course, such printing is largely predicated on the availability of precursors that smoothly and efficiently transform into high-quality films. In this contribution, we

*To whom correspondence should be addressed. E-mail: douglas.keszler@oregonstate.edu. Tel: +1-541-737-6736. Fax: +1-541-737-2062.

(1) Yuan, L.; Zhao, Y.-N.; Shang, G.-Q.; Wang, C.-R.; He, H.-B.; Shao, J.-D.; Fan, Z.-X. *J. Opt. Soc. Am. B* **2007**, *24*, 538.
(2) Goncalves, R. R.; Carturan, G.; Zampedri, L.; Ferrari, M.; Montagna, M.; Chiasera, A.; Righini, G. C.; Pelli, S.; Ribeiro, S. J. L.; Messaddeq, Y. *Appl. Phys. Lett.* **2002**, *81*, 28.
(3) Robertson, J. *Rep. Prog. Phys.* **2006**, *69*, 327.
(4) Wilk, G. D.; Muller, D. A. *Appl. Phys. Lett.* **2003**, *83*, 3984.
(5) Tang, C.; Tuttle, B.; Ramprasad, R. *Phys. Rev. B* **2007**, *76*, 073306.
(6) Cherkaoui, K.; Monaghan, S.; Negara, M. A.; Modreanu, M.; Hurley, P. K.; O'Connell, D.; McDonnell, S.; Hughes, G.; Wright, S.; Barklie, R. C.; Bailey, P.; Noakes, T. C. Q. *J. Appl. Phys.* **2008**, *104*, 064113.
(7) Zhong, L.; Zhang, Z.; Campbell, S. A.; Gladfelter, W. L. *J. Mater. Chem.* **2004**, *14*, 3203.
(8) Ohshita, Y.; Ogura, A.; Ishikawa, M.; Kada, T.; Hoshino, A.; Suzuki, T.; Machida, H.; Soai, K. *Chem. Vap. Deposition* **2006**, *12*, 130.
(9) Kuo, C. T.; Kwor, R.; Jones, K. M. *Thin Solid Films* **1992**, *213*, 257.
(10) Pereira, L.; Barquinha, P.; Fortunato, E.; Martins, R.; Kang, D.; Kim, C. J.; Lim, H.; Song, I.; Park, Y. *Thin Solid Films* **2008**, *516*, 1544.
(11) Lin, Y.-S.; Puthenkovilakam, R.; Chang, J.-P. *Appl. Phys. Lett.* **2002**, *81*, 2041.
(12) Swerts, J.; Peys, N.; Nyns, L.; Delabie, A.; Franquet, A.; Maes, J. W.; Elshocht, S. V.; Gendt, S. D. *J. Electrochem. Soc.* **2010**, *157*, G26.
(13) Kim, S.; Kim, J.; Choi, J.; Kang, H.; Jeon, H.; Bae, C. *J. Vac. Sci. Technol., B* **2006**, *24*, 1088.
(14) Aoki, Y.; Kunitake, T.; Nakao, A. *Chem. Mater.* **2005**, *17*, 450.

© 2011 American Chemical Society

describe a new water-based solution precursor for depositing HfO_2.

Thin film HfO_2 deposition through conventional sol−gel routes via spin coating or dip coating has been described in several reports. For example, hafnia sol precursors have been made by mixing $HfCl_4$ into ethanol or 1-methoxy-2-propanol followed by hydrolysis and peptization with acid.[15−17] Similar colloidal suspensions have been produced by using $HfOCl_2$ as the starting material.[2] Precursors have also been prepared by stabilizing hafnium ethoxide or hafnium pentadionate in acetylacetone/ethanol.[18−20] Each of these methods has relied on the preparation of large sol particles or use of a metal−organic reagent. Because of the high activation energy for interparticle densification and the incomplete expulsion of organic residues, these methods are predisposed to production of highly porous films. After annealing at 450 °C, refractive indices are commonly reported to be approximately 1.7 (λ = 550 nm), corresponding to a porosity >26%. Even though high-temperature annealing may facilitate densification of the deposited sols, it also leads to HfO_2 crystallization and grain boundary formation as annealing temperatures reach 500 °C. As insulators, these films exhibit high leakage current densities near 10^{-5} A/cm^2 at 1 MV/cm,[16,21] 3 orders of magnitude higher than that required for a thin film transistor (TFT) gate dielectric. To produce higher-quality material, a presumed surface sol−gel method has been described, which involves the use of a precursor of hafnium *n*-butoxide dissolved in toluene/ethanol.[14] In this method, an attempt is made to mimic the self-limiting reactions of ALD by inhibiting grain boundary, porosity, and cracking problems through sequential deposition of ultrathin layers. This approach, however, offers a slow deposition rate (0.6 nm/cycle), while associated island growth is manifested as surface roughness exceeding 1 nm.

In recent contributions, we have described a unique approach to the deposition of high-quality oxide films by using inorganic aqueous precursors. Examples include $HfO_{2-x}(SO_4)_x$ (HafSO*x*)[22] and $Al_2O_{3-3x}(PO_4)_{2x}$ (AlPO)[23] as dielectrics, ZnO[24] and $(InGaZn)_xO_y$[25] as semiconductors, and HafSO*x* as a directly imaged hardmask for writing sub-20 nm features.[26] These films exhibit properties comparable to those achieved via advanced vapor techniques. By promoting hydrolysis and condensation of metal species, while inhibiting the formation of large colloids, we converted wet precursor coatings smoothly to dense films. In this paper, we extend this approach to the preparation of a new precursor that enables unprecedented quality and thickness control for deposition of HfO_2 films from solution. The precursor chemistry allows a unique densification of the film, enabling its use as a high-performance dielectric. The dielectric performance is assessed both through capacitor and thin film transistor studies and correlated to the structural, morphological, and optical properties of the films.

Experimental Section

Precursor Synthesis. $HfOCl_2 \cdot 8H_2O$ (Alfa Aesar, 98+%) was dissolved in H_2O to a Hf concentration of 0.12 M. A total of 6.7 mL of 1 M NH_3(aq) (Mallinckrodt, ACS) was added to 20 mL of the solution with vigorous stirring (pH 8.5). The resulting precipitate was centrifuged and then washed with H_2O to remove Cl^- and ammonia. Rinse and separation steps were repeated five times until no precipitates were observed after mixing the supernatant with $AgNO_3$(aq). After these steps, the yield of Hf was measured to be 98%. Finally, 5 mL of 10 M H_2O_2(aq) (Mallinckrodt, ACS) and 1.4 mL of 2 M HNO_3(aq) (EDS, ACS) were added to the precipitates and stirred for approximately 12 h to obtain a clear precursor solution having pH 0.7. The final Hf concentration was 0.2 M with a NO_3^-/Hf ratio of 1.2. At room temperature, the precursor solution has been found to remain clear for at least one year. 18 MΩ Millipore water was used for each preparation.

Thin Film Deposition. Prior to deposition, all substrates were rinsed with H_2O followed by a 10 min ash in an O_2 plasma at 10 mTorr, 5 sccm O_2, and 0.75 W/cm^2. Films were deposited on substrates by spin coating, followed by an immediate hot plate cure at 150 °C for 1 min. This procedure was repeated until the desired thickness was obtained. A 1 h oven anneal in air at selected temperatures in the range 200−800 °C completed the process. For standard characterization, a 0.2 M Hf solution was spin coated at 3000 rpm for 30s, generating ∼8 nm/cycle after a final anneal at 400 °C. Film thickness for one deposition cycle could be readily adjusted in the range of 4−10 nm through precursor dilution and spin-coating parameters. Thicker coatings up to 40 nm were deposited after concentrating the standard precursor, though these films were not characterized extensively.

Structural and Chemical Characterization. For X-ray diffraction (XRD), transmission Fourier transform infrared (FT-IR), and electron probe microanalysis (EPMA) measurements, thin films were deposited on Si wafers coated with 200 nm of thermally grown SiO_2. XRD data were collected with a Rigaku RAPID diffractometer generating Cu Kα radiation. Transmission FT-IR spectra were collected on a Nicolet 5PC spectrometer with a bare Si/SiO_2 substrate as reference. EPMA data were obtained with a Cameca SX-50 with wavelength dispersive spectrometers and gas flow proportional detectors with P-10 gas. Intensities of O Kα, Si Kα, Cl Kα, N Kα, Hf Mα, and Zr Lα were collected at accelerating voltages of 8, 12, and 16 kV and averaged over 10 positions on each sample. Si, $Ca_5(PO_4)_3Cl$,

(15) Nishide, T.; Honda, S.; Matsuura, M.; Ide, M. *Thin Solid Films* **2000**, *371*, 61.
(16) Wang, K.-J.; Cheong, K.-Y. *Appl. Surf. Sci.* **2008**, *254*, 1981.
(17) Blanc, P.; Hovnanian, N.; Cot, D.; Larbot, A. *J. Sol-Gel Sci. Technol.* **2000**, *17*, 99.
(18) Villanueva-Ibanez, M.; Le Luyer, C.; Parola, S.; Marty, O.; Mungier, J. *Rev. Adv. Mater. Sci.* **2003**, *5*, 296.
(19) Zaharescu, M.; Teodorescu, V. S.; Gartner, M.; Blanchin, M. G.; Barau, A.; Anastasescu, M. *J. Non-Cryst. Solids* **2008**, *354*, 409.
(20) Blanchin, M. G.; Canut, B.; Lambert, Y.; Teodorescu, V. S.; Barau, A.; Zaharescu, M. *J. Sol-Gel Sci. Technol.* **2008**, *47*, 165.
(21) Wang, Z.-J.; Kumagai, T.; Kokawa, H.; Ichiki, M; Maeda, R. *J. Electroceram.* **2008**, *21*, 499.
(22) Anderson, J. T.; Munsee, C. L.; Hung, C. M.; Phung, T. M.; Herman, G. S.; Johnson, D. C.; Wager, J. F.; Keszler, D. A. *Adv. Funct. Mater.* **2007**, *17*, 2117.
(23) Meyers, S. T.; Anderson, J. T.; Hong, D.; Hung, C. M.; Wager, J. F.; Keszler, D. A. *Chem. Mater.* **2007**, *19*, 4023.
(24) Meyers, S. T.; Anderson, J. T.; Hung, C. M.; Thompson, J.; Wager, J. F.; Keszler, D. A. *J. Am. Chem. Soc.* **2008**, *130*, 17603.
(25) Meyers, S. T. Ph.D. Thesis, Oregon State University, 2008.
(26) Stowers, J.; Keszler, D. A. *Microelectron. Eng.* **2009**, *86*, 730.

BN, Hf, and Zr were used as standards. Raw intensities were corrected by a procedure detailed by Donovan and Tingle.[27] Elemental compositions were quantified by comparing experimental *k*-ratios to simulated values using StrataGEM thin film composition analysis software.

Morphology and Density. Thin films for scanning electron microscopy (SEM) and atomic force microscopy (AFM) were also deposited on Si/SiO_2 substrates. Thin films for X-ray reflectivity (XRR) were deposited on *p*-type Si substrates. Surface roughness was evaluated by using a Digital Instruments Nanoscope III Multimode atomic force microscope operated in contact mode with a Veeco NP-20 SiN_x probe at a scan frequency of 1.5 Hz. A low-pass filter and a second-order plane fit were applied to all samples to limit high-frequency noise and sample tilt. XRR data were collected with Cu Kα radiation (45 kV, 40 mA) on a Philips PW/3040 diffractometer. The incident beam was conditioned by using a 0.05 mm divergence slit. The exit beam was conditioned with a 0.1 mm detector slit. Low-angle reflections from 0.3° to 5° (2θ) were collected in 0.01° steps at 1 s/step. Analyses were conducted with X'Pert Reflectivity V1.0 software using sample thickness, surface roughness, and density as fitting parameters.

Optical Properties. HfO_2 films were spin coated on Si/SiO_2 substrates for spectroscopic ellipsometry (SE) measurements. Data were collected at the incident angles of 65°, 70°, and 75° in the range 300−1000 nm by using an HS-190 spectroscopic ellipsometer (J.A. Woolam Co.). SE provides the complex reflectance ratio $\rho = \tan(\Psi)\exp(i\Delta)$, where $\tan(\Psi)$ is the amplitude ratio upon reflection, and Δ is the phase difference. The ellipsometric data were analyzed by using the VASE software package. The analysis is based on least-squares regression analysis to obtain the unknown fitting parameters. Using appropriate optical models, the parameters were varied to minimize the difference between the calculated Ψ, Δ values, and the experimental data. The difference is represented by the mean square error (MSE). The transmission and reflection spectra from 390 to 850 nm were measured at near-normal incidence by using a double-grating spectrometer with a broadband Xe source and a Si photodiode detector. The thickness and wavelength-dependent refractive index, $n(\lambda)$, were obtained from analysis of the interference fringes in the reflection and transmission spectra.

Electronic Device Fabrication and Characterization. Metal−insulator−semiconductor (MIS) and metal−insulator−metal (MIM) capacitor test structures were constructed by spin coating HfO_2 thin films onto degenerate, *p*-type Si substrates (0.008−0.016 Ω cm) and onto Si wafers coated with 500 nm of Ta, respectively. The capacitors were completed by thermally evaporating 200 nm thick circular Al contacts via a shadow mask (0.011 cm^2) onto the annealed dielectrics. Relative dielectric constant and loss tangent were measured by using a Hewlett-Packard 4192A impedance analyzer. Leakage currents and breakdown fields were assessed by using a Hewlett-Packard 4140B picoammeter with a voltage ramp of 1 V/s. Bottom-gate thin film transistors were fabricated by rf sputtering through a shadow mask 50 nm of indium gallium zinc oxide (IGZO) channel materials onto 110 nm thick HfO_2 thin films on *p*-type Si substrates. HfO_2 films were produced via spin coating with a final anneal of 400 °C. Control devices were fabricated by depositing IGZO onto Si wafers having a 100 nm thick layer of SiO_2. The dielectric/semiconductor stacks were annealed at 300 °C for 1 h. Al source and drain contacts were thermally evaporated via a shadow mask; TFT dimensions were width = 1000 μm and length = 100 μm. The transistors were characterized in the dark with a Hewlett-Packard 4156C semiconductor parameter analyzer.

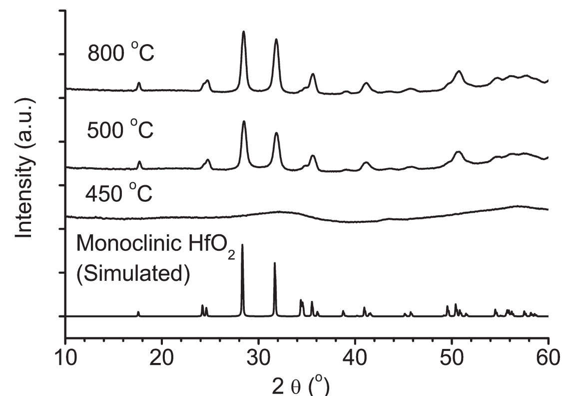

Figure 1. XRD patterns for films annealed at selected temperatures for 1 h.

Results and Discussion

The nature of the product HfO_2 films represents one of the more compelling aspects of the precursor chemistry. Therefore, we first describe the chemical and physical characteristics of the synthesized films. These qualities are further manifested through electrical test structures that incorporate these films. The nature of the precursor, which precedes the solid films, will then be discussed separately.

Thin Films. XRD data for films heated at temperatures up to 800 °C are illustrated in Figure 1. No discernible diffraction peaks are evident for films annealed at temperatures ≤450 °C for 1 h. As the temperature rises through and above 500 °C, the monoclinic form of HfO_2 crystallizes, persisting to the maximum temperature (800 °C) investigated. This crystallization behavior is similar to many conventional sol−gel derived films,[15,19,21] where the initial stage of crystallization has been observed near 450 °C via electron diffraction experiments.[19] Crystallization behavior of vapor-deposited films varies by deposition method and conditions. In some cases, as-deposited films from CVD,[8] sputtering,[10] and ALD[28] were observed to be polycrystalline.

FT-IR spectra were collected to monitor the hydration levels of films as a function of temperature. Spectra covering the energy range 2000−4000 cm^{-1} are illustrated in Figure 2. The primary absorption feature of interest is the broad band centered at approximately 3500 cm^{-1}, which is assigned to O−H stretching modes. The intensity of this band decreases significantly when the annealing temperature rises from 200 to 300 °C, indicating a major portion of the aqua and hydroxo groups are lost in this temperature range. The O−H absorption band is not observed after annealing the film at 500 °C, where the film crystallizes as HfO_2. Additionally, features associated

(27) Donovan, J. J.; Tingle, T. N. *J. Microsc. Soc. Am.* **1996**, *2*, 1.
(28) Hausmann, D. M.; Gordon, R. G. *J. Cryst. Growth* **2003**, *249*, 251.

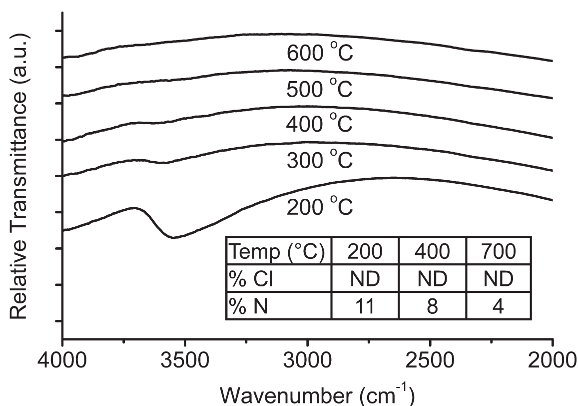

Temp (°C)	200	400	700
% Cl	ND	ND	ND
% N	11	8	4

Figure 2. FT-IR spectra of ~200 nm films and EPMA data with atomic percentages relative to Hf (inset). "ND" stands for "not detectable".

with nitrate absorption[29] at 1560 and 1280 cm^{-1} were clearly evident only for films annealed below 300 °C.

EPMA data were collected to further determine the residual counterion (Cl^- and NO_3^-) contents of the films (inset Figure 2). The measured Cl concentrations (< 0.5% relative to Hf) correspond to the noise threshold of the instrument for all the samples measured, supporting the chemical observations for AgCl precipitation that most of the Cl^- was removed through the precipitation, rinse, and centrifuge steps of the precursor synthesis. The atomic percentages of N range from approximately 10% to 4% with increasing temperatures. Recalling that the atomic ratio of NO_3^- to Hf is 1.2 in the precursor solution, it is apparent that a significant fraction of NO_3^- is eliminated during the deposition and subsequent annealing. For comparison, Southon and co-workers[30] heated a nitrate-based zirconia gel and determined most nitrate was lost by 400 °C, according to Raman spectroscopy. It is reasonable to assume that our rapidly converted thin films expel nitrate groups more readily. Quantifying the content of a light atom such as N via EPMA, however, is quite challenging; additional analytical techniques need to be applied to better quantify any NO_3^- residue or adsorbed N_2.

Surface and cross-section SEM images of films annealed at 400 and 600 °C are shown in Figure 3. The surface of the film annealed at 400 °C is so smooth that no features are discernible in the top-view SEM image (Figure 3a). The high-resolution cross-section SEM image (Figure 3b) reveals a continuous and dense film ~85 nm thick. For the crystallized film annealed at 600 °C, grain growth and grain boundary formation become apparent in both top-view and cross-section SEM images (Figure 3c, d). The thickness of this film is about 80 nm from Figure 3d. It is noteworthy that all films exhibit extreme smoothness and continuity without visible cracks and voids after experiencing the strong forces associated with drying and crystallization.

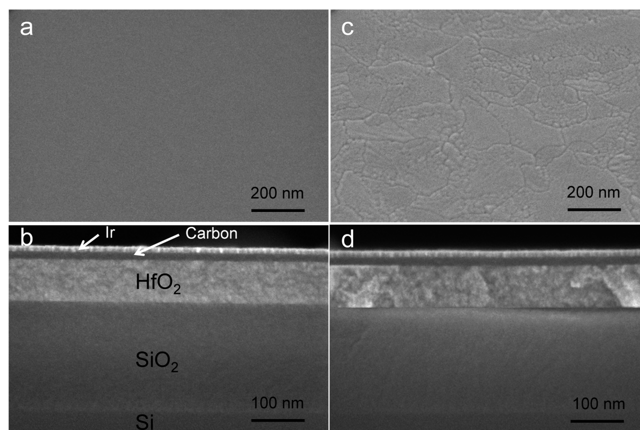

Figure 3. SEM images for films annealed at (a, b) 400 °C and (c, d) 600 °C for 1 h.

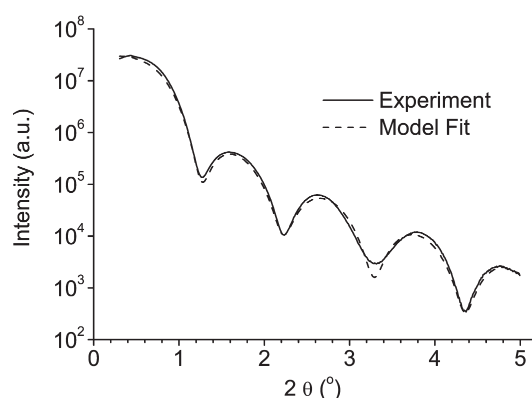

Figure 4. Experimental and modeled XRR patterns for an 8.3 nm film on Si annealed at 400 °C.

Consistent with the SEM results, contact-mode AFM imaging of films annealed below 500 °C reveals no distinguishable features of the films above the instrument noise floor, resulting in root-mean-square (rms) roughness values consistently ≤0.3 nm over a 2 μm × 2 μm area. Even for the well-crystallized film annealed as high as 800 °C, the roughness is only 0.7 nm.

XRR data were collected mainly to obtain film roughness and densities. For all films annealed in the range of 200−800 °C, Kiessig fringes in the patterns were found to extend beyond the maximum angle ($2\theta_{max}$ = 5°) set for the analysis. By fitting the experimental curves, we generated thicknesses, surface roughness, and density for each film. An XRR pattern for a 400 °C-annealed film, along with the model fit, is displayed in Figure 4 as an example of the data and model fit. Generated surface roughness and density following each temperature are plotted in Figure 5. The surface roughness for the film annealed at 200 °C is 0.25 nm, and it increases by approximately 0.15 nm as the annealing temperature increases to 500 °C. Above 500 °C, roughness increases sharply as grain growth is enhanced. The surface roughness values are consistent with those obtained from AFM measurements. The density increases significantly from 7.17 to 8.71 g/cm^3 as the annealing temperature rises from 200 to 400 °C and varies little at higher temperatures.

(29) Jose, J.; Bushiri, M. J.; Jayakumar, K.; Vaidyan, V. K. *AIP Conf. Proc.* **2008**, *1075*, 125.
(30) Southon, P. D.; Bartlett, J. R.; Woolfrey, J. L.; Stevens, M. G. *Ceram. Trans.* **1998**, *81*, 75.

Because the density evolution above 400 °C has not been thoroughly investigated, the precise density trend and potential maximum value cannot be inferred from Figure 5. Still, the value of 8.71 g/cm^3 for the 400 °C-annealed film corresponds to 86% of the single-crystal density of monoclinic HfO_2 (10.12 g/cm^3)[31] and is comparable to those reported (8.50 and 9.23 g/cm^3) for ALD HfO_2 films.[32,33] In contrast, from metal−organic-based solution precursors, corresponding ZrO_2 films achieved comparable relative densities only after annealing above 1000 °C, whereupon roughness increased dramatically.[34]

Ellipsometric data for 12-coat films were fit by modeling the bilayer HfO_2/SiO_2 with the parameters SiO_2 thickness (t_{SiO2}), HfO_2 thickness (t_{HfO2}), and Cauchy parameters A, B, and C for dispersion ($n(\lambda) = A + B/\lambda^2 + C/\lambda^4$) in the HfO_2 layer. Experimental and simulated ellipsometric spectra for a film annealed at 400 °C are shown in Figure 6. The fitting results for 300, 400, and 600 °C-annealed films, along with values of mean square error (MSE) are listed in Table 1. As shown in Figure 6,

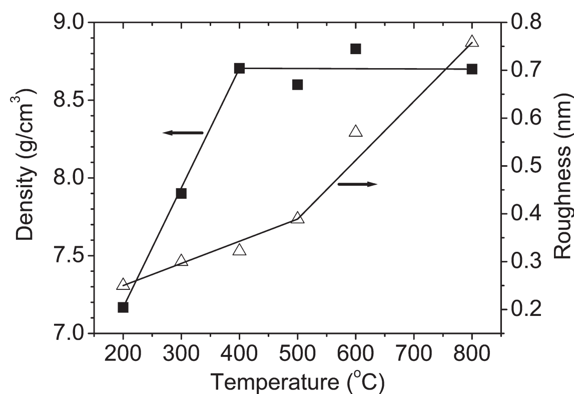

Figure 5. Temperature dependence of density and surface roughness examined via XRR.

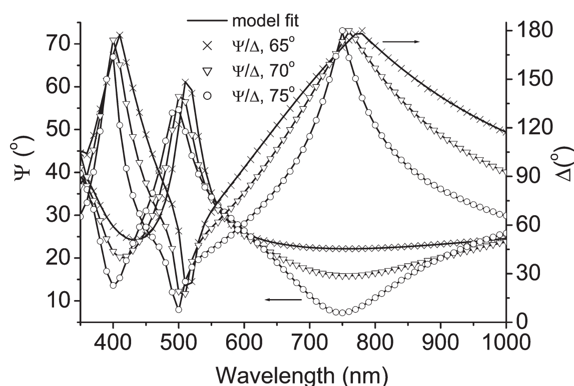

Figure 6. Experimental and modeled ellipsometric spectra represented by symbols and solid lines, respectively, for a 400 °C-annealed HfO_2/SiO_2 stack.

excellent agreement is achieved between the experimental data and the model, indicating that a homogeneous film has been produced. Because the derived values for the thickness of the SiO_2 layer are consistent with those observed from SEM images and the thermal growth conditions, we have a high level of confidence in the ellipsometric results. Also, as shown in Table 1, the film thickness shrinks by 13% between 300 and 400 °C anneals and little thereafter. The predominant change occurring by 400 °C is consistent with the general density trend generated from the XRR measurements (Figure 5).

Refractive index (n) dispersion curves obtained from the model fit are shown in Figure 7. The refractive indices at $\lambda = 550$ nm are 1.89, 1.92, and 1.93 for films annealed at 300, 400, and 600 °C, respectively. These high refractive indices are comparable to those for vapor-deposited HfO_2 films. For example, $n(550\text{ nm}) = 1.85 - 1.98$ and $n(633\text{ nm}) = 1.98$ have been reported for electron beam evaporated films and sputtered films, respectively.[35,36] The relative density of a film can be estimated by modeling the film as a combination of bulk material and a second phase (air or water) in void spaces via the effective optical medium approach represented by eq 1[37]

$$\frac{(n^2 - n_2{}^2)(n^2 + 2n_1{}^2)}{(n^2 + 2n_2{}^2)(n_1{}^2 - n^2)} = \frac{q_1}{1 - q_1} \qquad (1)$$

where n is the refractive index for the film, n_1 for bulk HfO_2 ($n_1 = 2.13$),[35] n_2 for voids in the form of air ($n_2 = 1$) or water ($n_2 = 1.33$), and q_1 is the volume fraction of the bulk. Because q_1 directly depends on n_2, the most physically reasonable second phase should be chosen. On the basis of the FT-IR results, voids composed of water are assumed for the 300 °C-annealed film and voids of air for the 400 and 600 °C-annealed films. Thus, bulk volume fractions of 77%, 88%, and 88% for 300, 400, and 600 °C-annealed films, respectively, are derived. These values agree well with the relative densities determined from XRR: 78%, 86%, and 87%. Alternatively assuming air voids at 300 °C generates a bulk fraction of 86%, while assuming water voids at 400 °C, gives a bulk fraction of 80%. These assumptions lead to large discrepancies with the results derived from XRR measurements. Therefore, FT-IR, XRR, and optical measurements are collectively consistent with the production of dehydrated and densified films after heating near 400 °C.

The refractive indices of ~260 nm thick films annealed in the range of 200−800 °C were also determined by fitting the thin film interference fringes in the reflection and transmission spectra. The $n(550\text{ nm})$ values determined by fringe fittings agree to within 1% of those by ellipsometric analyses.

Table 1. Model Fitting Results for Thickness of SiO_2 (t_{SiO2}) and HfO_2 (t_{HfO2}), HfO_2 Cauchy Parameters A, B, and C, and Mean Square Error (MSE)

anneal (°C)	t_{SiO2} (nm)	t_{HfO2} (nm)	A	B	C	MSE
300	201.3(3)	112.1(2)	1.854(2)	$8.6(9) \times 10^{-3}$	$4.7(9) \times 10^{-4}$	9.250
400	201.9(2)	97.6(1)	1.891(2)	$8.0(8) \times 10^{-3}$	$6.4(8) \times 10^{-4}$	8.106
600	202.7(2)	94.3(2)	1.901(2)	$7.3(9) \times 10^{-3}$	$6.3(9) \times 10^{-4}$	8.935

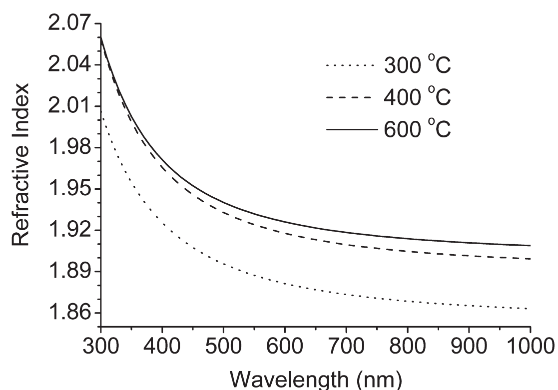

Figure 7. Dispersion of the refractive index of films following 1 h thermal anneals.

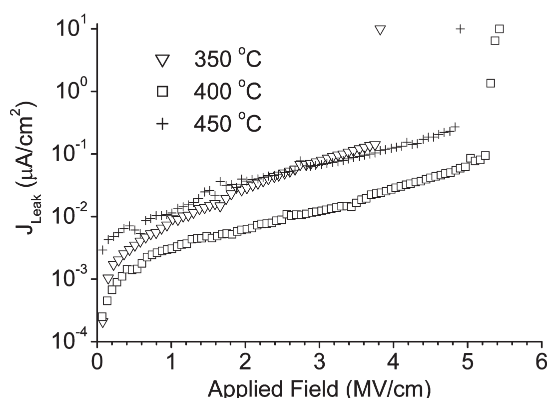

Figure 8. Representative current−voltage characteristics for films annealed in air for 1 h.

Table 2. Electrical Characteristics of MIS Capacitors with ∼120 nm HfO_2 Dielectrics Annealed in Air for 1 h

anneal (°C)	tan δ (%)	ε_r (1 kHz)	J_{Leak}[a] (nA/cm^2)	breakdown[b] (MV/cm)
300	9	13	5000	1.2 (CL)
350	0.8	12	10	3.5
400	0.7	12	3	5.5
450	0.7	13	5	4.5
500	5	13	67	2.9
600	6	13	N/A	0.8 (CL)

[a] J_{Leak} data were obtained at a field strength of 1 MV/cm. [b] CL stands for current-limited breakdown, which is defined as the field strength where leakage current density equals 10 μA/cm^2, when catastrophic and irreversible current events are not observed.

The dielectric properties of the films were first assessed by fabrication of MIS capacitor test structures, which were initially examined by small-signal capacitance and conductance measurements for determination of loss tangent (tan δ) and relative dielectric constant (ε_r) at 1 kHz. Results for films ∼120 nm thick and annealed at selected temperatures are summarized in Table 2. The relative dielectric constant is approximately 13 for films annealed in the range of 300 to 600 °C. The ε_r values for vapor-deposited HfO_2 films are reported to span the range 12−25.[10,11,32,38] The slightly higher dielectric constant for the films annealed at 300 °C compared with those annealed at 350 and 400 °C is attributable to residual, polarizable hydroxo groups; the high loss-tangent (9%) is also indicative of residual hydration in the films. Loss tangent values decrease to $<1\%$ for films annealed from 350 to 450 °C and then increase to $>5\%$ for films annealed at higher temperatures. The latter increase is associated with crystallization and the formation of grain boundaries. Current−voltage measurements on the same devices were used to evaluate dielectric breakdown. In cases where catastrophic and irreversible current increases were not observed, a current-limited breakdown is defined as the field strength where leakage current density exceeds 10 μA/cm^2. As shown in Table 2, the leakage current density is large for the 300 °C-annealed films. This result is once again related to incomplete dehydration. Catastrophic breakdown was observed for the thin film capacitors annealed in the range 350−450 °C (Figure 8). Here, all films demonstrated reliable breakdown of $\geq$3.5 MV/cm and leakage current densities of $\leq$10 nA/cm^2 at 1 MV/cm. Prior to breakdown, the small positive rise in current with increasing field may be associated with residual protons in the films. For films annealed at and above 500 °C, leakage current densities increase and breakdown fields decrease as crystallization occurs, grains grow, and grain boundaries develop (Figure 3c, d). To assess the reproducibility of the dielectric properties in MIM structures, identical films were cast on Ta-coated substrates with annealing temperatures of $\leq$350 °C. The results were found to be equivalent to those with the Si substrates. The performance of films as thin as 20 nm was also assessed on Si substrates. Average leakage current and breakdown of 12 nA/cm^2 and 4 MV/cm, respectively, were observed for films annealed at 400 °C.

TFTs were fabricated with solution-processed HfO_2 films as gate dielectrics and the amorphous oxide semiconductor indium gallium zinc oxide (IGZO) as active channels. TFT performance (Figure 9) was assessed through an analysis of the turn-on voltage (V_{on}), drain current on-to-off ratio (I_{on}/I_{off}), incremental channel mobility (μ_{inc}),[39] and subthreshold swing (S).[40]

As shown in the output curve (Figure 9a), qualitatively ideal transistor operation is evident from the field-effect current modulation (increasing I_D with increasing V_{GS}) and saturation in drain-to-source current at higher values of V_{DS}. As seen from the transfer curve (Figure 9b), the device exhibits strong current switching, represented by the small S value (0.30 V/dec) and high I_{on}/I_{off} ($>10^7$).

(31) Ruh, R.; Corfield, P. W. R. *J. Am. Ceram. Soc.* **1970**, *53*, 126.
(32) Conley, J. F., Jr.; Ono, Y.; Tweet, D. J.; Zhuang, W.; Solanki, R. *J. Appl. Phys.* **2003**, *93*, 712.
(33) Hausmann, D. M.; Kim, E.; Becker, J.; Gordon, R. G. *Chem. Mater.* **2002**, *14*, 4350.
(34) Lenormand, P.; Lecomte, A.; Babonneau, D.; Dauger, A. *Thin Solid Films* **2006**, *495*, 224.
(35) Jerman, M.; Qiao, Z.; Mergel, D. *Appl. Opt.* **2005**, *44*, 3006.
(36) Martinez, F. L.; Toledano-Luque, M.; Gandia, J. J.; Carabe, J.; Bohne, W.; Rohrich, J.; Strub, E.; Martil, I. *J. Phys. D: Appl. Phys.* **2007**, *40*, 5256.
(37) Mergel, D. *Thin Solid Films* **2001**, *397*, 216.
(38) Rauwel, E.; Clavel, G.; Willinger, M. G.; Rauwel, P.; Pinna, N. *Angew. Chem.* **2008**, *120*, 3648.
(39) Hoffman, R. L. *J. Appl. Phys.* **2004**, *95*, 5813.
(40) Schroder, D. K. Semiconductor Materials and Device Characterization, 2nd ed.; John Wiley and Sons: New York, 1998.

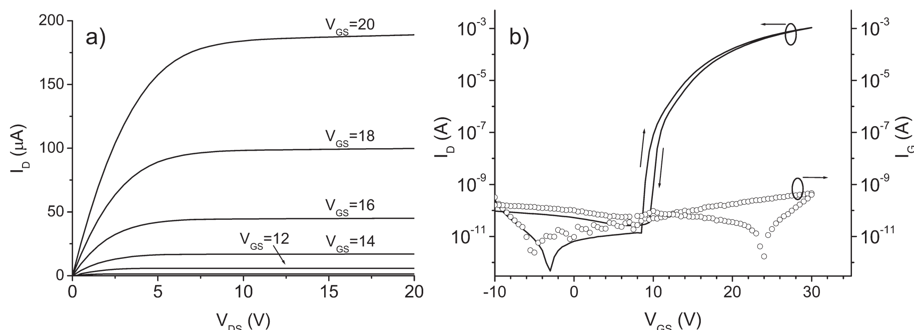

Figure 9. Representative (a) $I_D - V_{DS}$ (b) $\log(I_D) - V_{GS}$ (V_{DS} = 10 V) and $\log(I_G) - V_{GS}$ curves for a TFT with a HfO_2 gate dielectric and a sputtered IGZO channel. (V_{GS} is stepped from 6 to 20 V in 2 V increments for the $I_D - V_{DS}$ curve.).

Calculation of μ_{inc} from the transconductance yielded a peak value of 13.1 $cm^2/V \cdot s$ at V_{GS} = 25 V. Notably, the gate dielectric exhibits very low leakage current (< 1 nA) even as the drive current reaches mA levels, consistent with the performance of the HfO_2 films in the MIS and MIM capacitors. The device exhibits V_{on} = +8.5 V, higher than that (V_{on} = +2 V) for a SiO_2 control dielectric. We attribute this relatively large value of V_{on} to electron-trapping states at the semiconductor–insulator interface, which may arise from plasma damage of the films during sputter deposition of IGZO. Such traps also contribute to the clockwise 1 V hysteresis in the transfer curve.

Precursor. A flow diagram representing the primary steps in the synthesis of the precursor is depicted in Scheme 1. In Step (1), the reagent $HfOCl_2 \cdot 8H_2O$ is simply dissolved in water. It has been well established that this dissolution preserves the tetrameric species, $Hf_4(OH)_8(H_2O)_{16}^{8+}$.[41–44] The tetramer consists of four metal atoms at the corners of a square plane and doubly bridged by hydroxo ligands. Rapid addition of NH_3(aq) induces hydrolysis and condensation, leading to a gelatinous precipitate. Other researchers have precipitated zirconia nuclei of 15–30 Å after refluxing/modest drying.[45–47] Our rapidly induced precipitation conditions favor nearly amorphous precipitates; assuming only modest particle growth during centrifuging and washing, ordered regions of ≤2 nm in diameter are expected. The basic square structure of the tetramer is preserved during condensation by olation.[45,48] Thin film EPMA measurements, *vide supra*, revealed the absence of Cl^- in the films. Hence, the centrifuge and wash procedures effectively remove Cl^- from the solutions. The overall process of precipitation, centrifugation, and washing, is summarized as Step (2). By adding HNO_3(aq) at approximately one mole equivalent with respect to Hf, the precipitate can be completely dissolved. Considering the weak complexing ability of NO_3^- toward Hf,[49] and assuming the tetrameric structure remains intact, we propose the general formula $[Hf_4(OH)_{12} \cdot yH_2O]_m^{4m+}$ for the species existing after dissolution of the precipitate with HNO_3(aq). The value of "*y*" represents a level of hydration different from that of the precipitate. The value of "*m*" is less than about 30 on the basis of nuclei no larger than 2 nm. This dissolution, as Step (3a), is further represented by the reaction of eq 2, where for clarity, the formulas of the Hf species are simplified.

Scheme 1. Flow Diagram for HfO_2 Precursor Preparation

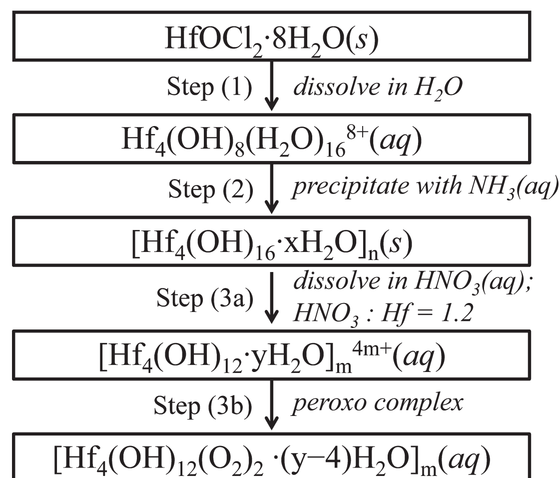

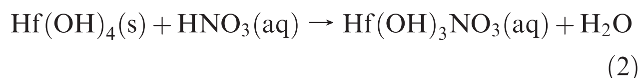

$$Hf(OH)_4(s) + HNO_3(aq) \rightarrow Hf(OH)_3NO_3(aq) + H_2O \quad (2)$$

Dissolution of the precipitate with HNO_3(aq), however, is quite slow, requiring up to two weeks. Simultaneous addition of H_2O_2(aq) shortens this time to approximately 12 h, indicating that the peroxo group plays an important role in dissociating aggregated particles and species by coordinating to Hf. We have found that the precursors containing peroxide also produce much more uniform films than those containing only nitrate. Moreover, it has been demonstrated that the low energies required for decomposition of the peroxo

(41) Johnson, J. S.; Kraus, K. A. *J. Am. Chem. Soc.* **1956**, *78*, 3937.
(42) Zielen, A. J.; Connick, R. E. *J. Am. Chem. Soc.* **1956**, *78*, 5785.
(43) Toth, L. M.; Lin, J. S.; Felker, L. K. *J. Phys. Chem.* **1991**, *95*, 3106.
(44) Aberg, M.; Glaser, J. *Inorg. Chim. Acta* **1993**, *206*, 53.
(45) Clearfield, A. *Rev. Pure Appl. Chem.* **1964**, *14*, 91.
(46) Keramidas, V. G.; White, W. B. *J. Am. Ceram. Soc.* **1974**, *57*, 22.
(47) Matsui, K.; Suzuki, H.; Ohgai, M. *J. Am. Ceram. Soc.* **1995**, *78*, 146.
(48) Clearfield, A. *J. Mater. Res.* **1990**, *5*, 161.
(49) Colfen, H.; Schnablegger, H. *Langmuir* **2002**, *18*, 3500.
(50) Jiang, K.; Zakutayev, A.; Stowers, J.; Anderson, M. D.; Tate, J.; McIntyre, D. H.; Johnson, D. C.; Keszler, D. A. *Solid State Sci.* **2009**, *11*, 1692.
(51) Connick, R. E.; McVey, W. H. *J. Am. Chem. Soc.* **1949**, *71*, 3182.

ligands enable prompt condensation during the formation of the film and consequently low-temperature densification.[26,50] Hence, the introduction of peroxide into the precursor solution provides substantial benefits.

Unlike the well-established peroxo chemistry of the early transition elements Ti, V, Nb, Mo, and W, the corresponding chemistry of Hf and Zr is less developed. From equilibrium studies, coordination of the peroxo ligand to Zr in $HClO_4$(aq) was proposed as early as 1949.[51] In more recent studies, the Zr:peroxide ratio in the same system was determined to be 2:1 by titration methods.[52] We also note a recent report of a ZrO_2 precursor prepared by dissolving $ZrO(NO_3)_2$ in a mixture of H_2O_2(aq) and NH_3(aq) for thin film deposition.[53] On the basis of our calculations using the Partial Charge Model (PCM)[54] (Supporting Information), we find peroxo complexing to Hf is possible during the dissolution process, as depicted as Step (3b) in Scheme 1.

All the aforementioned chemical interactions are critical design elements for this thin film precursor. Precipitates are created rapidly, and despite their inherently high reactivity, are separated and solvated with peroxide and minimal acid. Nanoparticles are stabilized without the use of bulky organic complexing ligands so that the precursor can be converted to solid with minimal disruption. Results of speciation studies on the precursor solutions will be described in forthcoming contributions.

Summary and Perspective

A new aqueous precursor has been designed for the atmospheric deposition of atomically smooth and dense thin films of HfO_2. Ligands and their concentrations have been chosen to carefully control ionic strength and condensation reactions. As a result, a precursor is realized that exhibits both an extended shelf life as well as low-energy pathways to densification. The present demonstration by spin coating is inherently planarizing, though surface mediated growth techniques may enable conformal coating by the same precursor. The properties of the derived films substantively exceed those produced by any other solution technique and in most respects rival those produced via advanced vapor methods. The chemical and structural characteristics of the films in the temperature range of 300−450 °C are truly unique to this process, especially with respect to the interplay between hydration and crystallization. Results of continued fundamental studies are likely to have many implications for application of the materials across several different platforms. Clearly, the present results represent substantive progress toward developing the robust materials sets that will be required to realize a high-performance printed macroelectronics technology. At the same time, understanding the nature of the molecular species in the aqueous solutions will provide greater control over the early stages of condensation and dehydration.

Acknowledgment. We thank Andriy Zakutayev for assistance with the optical transmission/reflection measurements and the Hewlett-Packard Company for use of the SEM. This research was supported by the National Science Foundation Grant CHE-0847970 (J.T.A., D.A.K., J.F.W.), the Air Force Research Lab (K.J.), and the Hewlett-Packard Company (K.H.).

Supporting Information Available: Partial Charge Model calculation. This material is available free of charge via the Internet at http://pubs.acs.org.

(52) Thompson, R. C. *Inorg. Chem.* **1985**, *24*, 3542.
(53) Gao, Y.; Masuda, Y.; Ohta, H.; Koumoto, K. *Chem. Mater.* **2004**, *16*, 2615.
(54) Henry, M.; Jolivet, J. P.; Livage, J. *Struct. Bonding* (*Berlin, Ger.*) **1992**, *77*, 153.